Asymmetry in the Elastic Scattering of Polarized Protons by Deuterium*†

STEWART M. MARCOWITZ
The Enrico Fermi Institute for Nuclear Studies and Physics Department, The University of Chicago, Chicago, Illinois
(Received June 3, 1960)

Asymmetries in the elastic scattering of polarized protons by deuterium have been measured at 419 Mev at proton center-of-mass angles from 47.9° to 115°. The inferred polarizations are -0.092 ± 0.058 at 47.9°, -0.502 ± 0.058 at 59°, -0.583 ± 0.081 at 68°, -0.141 ± 0.056 at 77.8°, -0.122 ± 0.111 at 90°, -0.150 ± 0.059 at 97°, -0.309 ± 0.073 at 105°, and $+0.174\pm0.059$ at 115°. It is suggested that using the impulse approximation these results may serve as a test of nucleon-nucleon scattering phase shifts or, with proton-proton scattering data, may be used to obtain $I=0$ nucleon-nucleon phase shifts.

1. INTRODUCTION

IT has been suggested[1] that the polarization of nucleons elastically scattered by deuterons can be used as a test of nucleon-nucleon (N-N) scattering phase shifts. The polarization of protons elastically scattered by deuterium (p-d) may be used instead of neutron-proton (n-p) polarization to obtain a best set of N-N phase shifts. The p-d polarization $P(\bar{\theta})$ as a function of p-d center-of-mass angle $\bar{\theta}$ is given in the impulse approximation[2] by

$$P(\bar{\theta})=\frac{16}{9I(\bar{\theta})}\{2\ \mathrm{Re}\Lambda_2^*(\Lambda_1+\tfrac{2}{3}\Lambda_5)\}, \tag{1}$$

where

$$I(\bar{\theta})=(16/9)\{|\Lambda_1|^2+|\Lambda_2|^2+\tfrac{2}{3}(|\Lambda_2|^2+|\Lambda_3|^2+|\Lambda_4|^2+|\Lambda_5|^2)\}, \tag{2}$$

and

$$\Lambda_i=(\lambda_i{}^{pp}+\lambda_i{}^{pn})S(\mathbf{q}). \tag{3}$$

q is the magnitude of the momentum transfer;

$$S(\mathbf{q})=\int\Psi^2(\mathbf{r})\exp[i\tfrac{1}{2}\mathbf{q}\cdot\mathbf{r}]d\tau. \tag{4}$$

$\Psi(\mathbf{r})$ is the deuteron wave function. The λ_i are coefficients in the N-N scattering matrix

$$m=\lambda_1+\lambda_2(\boldsymbol{\sigma}_1+\boldsymbol{\sigma}_2)\cdot\mathbf{n}'+\lambda_3(\boldsymbol{\sigma}_1\cdot\mathbf{K}')(\boldsymbol{\sigma}_2\cdot\mathbf{K}')+\lambda_4(\boldsymbol{\sigma}_1\cdot\mathbf{p}')(\boldsymbol{\sigma}_2\cdot\mathbf{p}')+\lambda_5(\boldsymbol{\sigma}_1\cdot\mathbf{n}')(\boldsymbol{\sigma}_2\cdot\mathbf{n}'), \tag{5}$$

where the orthogonal unit vectors $\mathbf{n}'$, $\mathbf{p}'$, and $\mathbf{K}'$ are given by

$$\mathbf{n}'=\frac{\mathbf{k}_0'\times\mathbf{k}'}{|\mathbf{k}_0'\times\mathbf{k}'|},\quad \mathbf{p}'=\frac{\mathbf{k}_0'+\mathbf{k}'}{|\mathbf{k}_0'+\mathbf{k}'|},\quad \text{and}\quad \mathbf{K}'=\frac{\mathbf{k}'-\mathbf{k}_0'}{|\mathbf{k}'-\mathbf{k}_0'|}. \tag{6}$$

$\mathbf{K}_0'$ and $\mathbf{k}'$ are the initial and final momenta of the incident nucleon and $\boldsymbol{\sigma}_1$, $\boldsymbol{\sigma}_2$ the spins of the incident and target nucleons, respectively. The Λ_i depend on the p-d center-of-mass momentum $\mathbf{k}$ and scattering angle $\bar{\theta}$, and the λ_i depend on the corresponding N-N variables $\mathbf{k}'$ and $\bar{\theta}'$, such that the momentum transfer $\mathbf{q}$ is the same in both cases. This leads to the kinematic requirements

$$k'=\tfrac{3}{4}k,\quad \sin(\bar{\theta}'/2)=\tfrac{4}{3}\sin(\bar{\theta}/2), \tag{7}$$

and $\mathbf{K}$, $\mathbf{p}$, and $\mathbf{n}$ are along $\mathbf{K}'$, $\mathbf{p}'$, and $\mathbf{n}'$, respectively. Combining Eqs. (1) through (7), it is seen that $P(\bar{\theta})$ is independent of the detailed deuteron wave function. The detailed dependence of the λ_i on the N-N phase shifts is shown in the Appendix.

Given a complete set of N-N phase shifts,[3–6] the polarization of protons elastically scattered from deuterium can be computed and can be compared with the experimentally determined polarization. An alternative is to use the experimentally determined p-d polarization and a set of proton-proton (p-p) phase shifts[7] to obtain a set of equations in which the $I=0$ phase shifts appear as variables. Then in principle, these equations could be solved for the $I=0$ phase shifts. It should be noted that the kinematic requirements of this analysis do not permit the computation of the polarization beyond an angle of 97° in the center-of-mass system. However, the impulse approximation is not expected to be valid at very large angles. At present, there are no experimentally determined high-energy $I=0$ phase shifts. Attempts have been made to measure the n-p scattering at 310 Mev[6] and at 350 Mev.[8] At 310 Mev, a polarized proton beam was scattered by a liquid deuterium target and the high-energy neutrons were observed. It was assumed that the polarization from the bound neutron in deuterium is equivalent to the polarization from a free neutron. This has been subsequently shown not to be

* This research was supported by a joint program of the Office of Naval Research and the U. S. Atomic Energy Commission.
† A thesis submitted to the Department of Physics, the University of Chicago, in partial fulfillment of the requirements for the Ph.D. degree.
[1] L. Castillejo and L. S. Singh, Nuovo cimento **11**, 131 (1959).
[2] G. F. Chew, Phys. Rev. **80**, 196 (1950); **84**, 710, 1057 (1951).
[3] J. L. Gammel and R. M. Thaler, Phys. Rev. **107**, 291 (1957); J. L. Gammel and R. M. Thaler, Phys. Rev. **107**, 1337 (1957).
[4] P. S. Signell and R. E. Marshak, Phys. Rev. **109**, 1229 (1958).
[5] N. Metropolis, H. P. Stapp, and T. J. Ypsilantis, Phys. Rev. **105**, 302 (1957); H. A. Bethe, Ann. Phys. **3**, 190 (1958).
[6] O. Chamberlain, E. Segrè, R. D. Tripp, C. Wiegand, and T. J. Ypsilantis, Phys. Rev. **105**, 288 (1957). Note that there are some errors in the coefficients in this paper.
[7] M. H. MacGregor, M. J. Moravcsik, and H. P. Stapp, Phys. Rev. **116**, 1248 (1959).
[8] R. T. Siegel, A. J. Hartzler, and W. A. Love, Phys. Rev. **101**, 838 (1956).

the case.[9] At 350 Mev the n-p scattering was done directly. However, serious difficulties with the neutron beam are evident. Agreement has been claimed between these two results but neither have been subjected to phase-shift analysis. The inherent difficulties involved in obtaining high-intensity, monoenergetic, highly polarized neutron beams coupled with the difficulty in monitoring, impossibility of focusing, and intrinsic inefficiencies in detecting neutrons indicate that the p-d polarization may be the best way to obtain the $I=0$ phase shifts. The measurement of the elastic p-d polarization has been attempted previously.[10] However, low beam intensity ($\sim$1000 protons/inch^2 sec), the difficulty in separation of elastic from inelastic events, and the large detector size made the angular and polarization statistics poor (Fig. 11). A measurement of the high-energy elastic p-d polarization is, therefore, desirable. At present there are no satisfactory N-N phase shifts available at 420 Mev. A ready test for them when they do become available will be very useful.

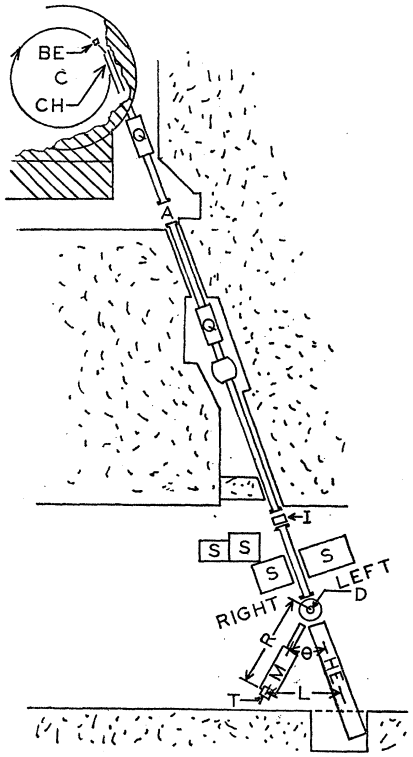

FIG. 1. Plan view of the experimental setup. Cyclotron, C; internal beryllium target for polarizing the beam, BE; extraction channel, CH, which accepts only protons scattered at a small angle to the left; strong-focus magnets, Q; air gap for inserting absorber to degrade the beam energy, A; ionization chamber monitor, I; shielding blocks, S; liquid deuterium target, D; spectrometer magnet, M; counter telescope, T; helium-filled polyethylene bag to reduce air scattering from the direct beam, HE; the distance from the target center to a pointer index mounted on the spectrometer (164 inches), R; the chord length between the beam center and the pointer, L; the scattering angle, θ. Right and left directions are indicated.

2. EXPERIMENTAL ARRANGEMENT (FIG. 1)

In the experiment described here a (61.5±1.5)% polarized 419±3.5 Mev proton beam[11] of intensity 2×10^7 protons/second extracted from the University of Chicago synchrocyclotron (C) was used. The beam passed through an ionization chamber (I) monitor after being focused and was scattered by a liquid deuterium target (D). The scattered particles passed through a vertically deflecting magnetic spectrometer[12] (M) which could be rotated about the target. After the spectrometer, the scattered particles entered a quadruples counter telescope (T) where they were counted. Most of the path was through 6-inch diameter vacuum pipes. The counters were shielded from the direct beam line and beam stop by concrete shielding blocks (S). Lead was stacked around the counter telescope to further reduce the background. A 20-foot long, 2-foot diameter polyethylene bag (HE) filled with helium was placed in the beam line after the liquid deuterium target to reduce background from the beam scattering in the air.

3. BEAM

The beam was obtained by elastically scattering 450-Mev protons internally from a beryllium target (BE) at an angle of about 13.5° to the left. The beam was then extracted through a magnetic channel (CH). Focusing was achieved by a set of quadrupole strong-focusing magnets (Q).

The mean energy of the beam was determined from a Bragg curve (Fig. 2). For this measurement, two scintillation counters in coincidence were used as monitors. Copper absorbers were placed between the counters and an ionization chamber. The charge, in arbitrary units per incident proton, plotted against the thickness of absorber gives the Bragg curve. The point which is 82%[13] of the peak height corresponds to the unrectified mean range (R^*). The mean range R is given by $(R-R^*)/R=Z/6400$. R^* was 129.4 g/cm^2 of copper. R is then 130 g/cm^2, which gives a mean beam energy[14] of 419 Mev. The energy spread of the beam was determined from the momentum profile of the beam (Fig. 3). The direct beam was monitored by two scintillation counters in coincidence and was momentum analyzed by passing through the magnetic spectrometer. The number of protons with a given momentum was counted for a fixed number of incident protons by means of a triples coincidence telescope at the exit of the magnet. By varying the magnet current, and hence the momentum, the momentum profile of

[9] R. J. N. Phillips, Proc. Phys. Soc. (London) **74**, 652 (1959).
[10] J. Marshall, L. Marshall, D. Nagle, and W. Skolnik, Phys. Rev. **95**, 1020 (1954).
[11] R. H. March, Chicago Synchrocyclotron internal report (unpublished).
[12] A. V. Crewe, Rev. Sci. Instr. **29**, 880 (1958).
[13] R. Mather and E. Segrè, Phys. Rev. **84**, 191 (1951).
[14] M. Rich and R. Madey, University of California Radiation Laboratory Report UCRL-3301, 1954 (unpublished).

the beam was obtained. The beam momentum profile has a full width at half maximum of 2.7%. The magnet and counter telescope were known to have a resolution of 1.4% in momentum. The beam then had a momentum spread of 2.3% or an energy spread of 1.6%. The beam energy was, therefore, 419±3.5 Mev.

4. BEAM MONITOR

The ionization chamber which was used as a monitor in the experiment is known to be accurate to 2%. The charge was integrated by a vibrating-reed electrometer and was observed on a multiple-range Brown recorder. A switching circuit connected to the Brown recorder controlled the scalars so that they counted automatically for a fixed number of incident protons.

5. BEAM POLARIZATION

The beam polarization (P_1) was accurately determined in a previous cyclotron run[15] from the asymmetry (ϵ) in a second scattering from a beryllium target at angles ranging from 11° to 15°. The asymmetry was shown to be constant over this range. The techniques used in measuring asymmetries to determine the beam polarization at that time are the same as those which were used in the present experiment:

$$\epsilon = P_1 P_2 = (L-R)/(L+R). \quad (8)$$

P_2 is the polarization in the second scattering. L and R are the intensities of protons scattered to the left and right, respectively, in arbitrary units. In the measurement of the beam polarization, $P_1 = P_2$, and $\epsilon = P_1^2$. P_1 averaged over numerous measurements was (61.5 ±1.5)%. There are grooved marks in the cyclotron vacuum tank which permit the magnetic channel to be removed and installed again in exactly the same position at later times. The beryllium target is fixed permanently to the magnetic channel. The angular beam spread accepted by the magnetic channel is very small. It is well known that the polarization is essentially constant over a large range of angles[16] including those accepted by the magnetic channel. It can then be confidently said that the polarization in this experiment was the same as in the previous run. A very rough measurement at the end of the present run gave a polarization of approximately the same magnitude.

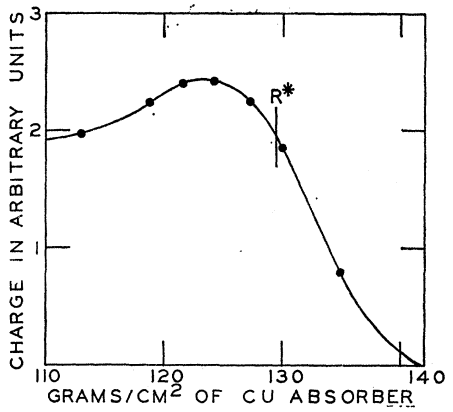

FIG. 2. Bragg curve. The mean rectified range R is obtained from R^* (82% of the maximum) by $(R-R^*)/R = Z/6400$. The mean energy was 419 Mev.

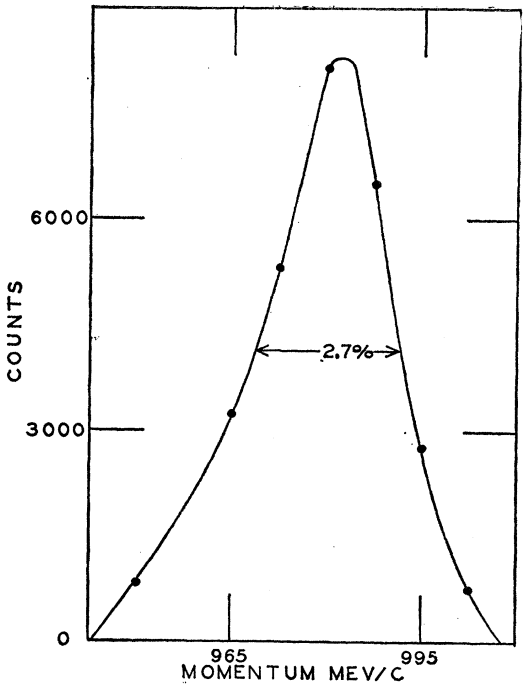

Fig. 3. Beam momentum profile. After taking into account the 1.4% resolution of the magnet and counter telescope the beam energy spread is 7 Mev.

Knowing the polarization (P_1) in the first scattering, the polarization (P_2) in a second scattering can be inferred from the asymmetry ($\epsilon = P_1 P_2$).

6. BEAM CENTER

The beam line was first roughly determined by photographs. The magnetic spectrometer was set approximately on the beam line. The magnet position was measured by means of a pointer mounted on the magnet near the floor. This pointer was 164 inches from the target position (R) (see Fig. 1). The direct beam, reduced in intensity, monitored by two scintillation counters in coincidence, was allowed to pass through the magnetic spectrometer and register in a triples counter telescope. The number of counts for a fixed number of incident protons was measured as a function of magnet current. The momentum profile of the beam is such a curve. Setting the magnet at a current corresponding to the peak of the beam mo-

[15] R. H. March, University of Chicago Report, EFINS-343 (1960), (to be published).

[16] H. G. de Carvalho, J. Marshall, and L. Marshall, Phys. Rev. 96, 1081 (1954).

mentum profile, the magnet was shifted in position in $\frac{1}{2}$-inch steps. The number of counts, for the same number of incident protons, at the peak momentum of the beam, measured at each position, gives the beam position profile (Fig. 4). The curve has a full width at half maximum of 3 inches. This indicates that the beam was larger than the effective aperture of the magnet, which accounts for the fact that the beam position profile is not flat-topped. From the beam position profile the beam center was determined to $\frac{1}{4}$ inch. A beam photo after the liquid deuterium target showed the beam as a spot $1\frac{1}{2}$ inches in diameter.

7. ANGLE MEASUREMENTS

Angles were obtained by measuring the chord length (L) (see Fig. 1) from the beam center to the pointer on the magnet. Knowing the distance (R) from the target to the pointer on the magnet, the angle (θ) was calculated: $L/2=R\sin(\theta/2)$. L could be measured to $\frac{1}{4}$ inch; $\Delta L/2R=\Delta\sin(\theta/2)\sim\Delta(\theta/2)$. From this it is seen that angles could be measured to 0.09°. The $\frac{1}{4}$-inch uncertainty in the beam position introduced another 0.09°. Angles were then determined to 0.12°. The angular aperture of the entrance slit of the magnet was 0.75°. Accuracy in angle measurements had added importance because of the rapid change of the differential elastic p-d cross section[17] with angle.

8. LIQUID DEUTERIUM TARGET (FIG. 5)

The liquid deuterium target was made by modifying an already existing liquid hydrogen target[18,19] so that deuterium gas could be liquified in it. The actual target (T) was an upright Mylar cylinder $4\frac{1}{2}$ inches high, $3\frac{3}{4}$ inches in diameter, with brass top and botton. The liquid deuterium thickness was about 1.4 g/cm^2. The surrounding vacuum tank (J) had a 12-mil thick aluminum window (AL). Both the entering and scattered beam had to pass through this window. Inside the vacuum tank, the target was also surrounded by a $\frac{1}{2}$-mil gold-plated Mylar heat shield (MR). This heat shield was transparent to visible light. With the aid of a Lucite light pipe (L) through the vacuum jacket, the target could be illuminated and the liquid level in the target could be observed visually through the $2\frac{3}{4}$-inch square, Mylar, direct beam exit window. The liquification chamber (D_2) above the target was also designed to be used as a reservoir for the liquid deuterium during empty target measurements. The liquid could be forced out of the target by a applying a small gas pressure at the liquid surface in the target. Unfortunately, the deuterium lines became plugged early in the experiment and the target could not be emptied until the end of the experiment. Since empty target subtractions could not be made, accurate measurements of backgrounds and base line determinations were necessitated to eliminate the effect of the target container. This will be discussed later. The deuterium used was the same as that used in reference 10. It was experimentally evident that the hydrogen contamination was worse than the 2% quoted in reference 10. The effect of this contamination will be discussed later.

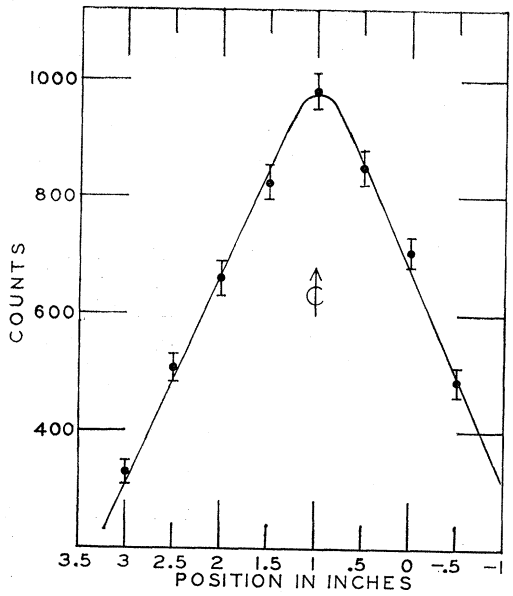

FIG. 4. Beam position profile. The beam center was determined to 0.25 inch which at 164 inches from the target is less than 0.1 degree.

9. COUNTER TELESCOPE (FIG. 6)

The counter telescope [Fig. 6(a)] consisted of four 6-inch long plastic scintillation counters placed at the magnet exit. These are called 1, 2, 3, and 4, respectively. Counters 1, 2, and 4 were looked at, end on, by two 1P21 photomultiplier tubes, the pulses of which were added. Counter 3 was looked at, end on, by two 6810A photomultiplier tubes. Provision was made for splitting the 6810A pulses and adding the split pulses independently. Half of the counter-3 pulse was used for coincidence purposes, the other half was used for pulse-height analysis. Counter 1 was a $\frac{1}{2}$-inch wide defining counter $\frac{1}{8}$ inch thick in the direction of the beam. Counter 2 was $\frac{3}{4}$ inch wide by $\frac{1}{8}$ inch thick. Counter 3 was 1 inch wide by $\frac{3}{8}$ inch thick. Counters 1, 2, and 3 were used in fast coincidence. Counter 4 was $1\frac{1}{2}$ inches wide by $\frac{1}{4}$ inch thick and was usually used in anticoincidence with counters 1, 2, and 3. An absorber tray permitted the installation of absorbers between counters 3 and 4 for range separations. The resolution of the coincidence circuits used was 10 mμsec.

The geometry was such that measuring voltage plateaus for counters 2, 3, and 4 was actually an efficiency measurement. These counters were made

[17] A. V. Crewe, B. Ledley, E. Lillethun, S. M. Marcowitz, and L. G. Pondrom, Phys. Rev. **114**, 1361 (1959).
[18] R. C. Arnold and U. E. Kruse, Chicago Synchrocyclotron internal report (unpublished).
[19] U. E. Kruse and R. C. Arnold, Phys. Rev. **116**, 1008 (1959).

essentially 100% efficient. Used in anticoincidence, counter 4 was shown to be 99% efficient. A well-defined plateau was obtained for counter 1 which indicated that it too was 100% efficient. After the proper voltage and delay settings had been determined and set, the selection of particles was done as follows. The magnetic spectrometer separated out charged particles of a particular momentum. Enough absorber to stop deuterons of this momentum, but not enough to stop the corresponding protons, was placed between counters 3 and 4. Two scalars [Fig. 6(b)] were used, one to count $123\bar{4}$ coincidences and another to count 123 coincidences. A $123\bar{4}$ coincidence was the signature of a deuteron. Both deuterons and protons gave 123 coincidences so that proton counts were obtained from $123 - 123\bar{4}$. In addition, 123 coincidences were introduced by cosmic rays. The telescope was inclined at 60° with the horizontal. Since the counting times were frequently long, this amounted to a rather large correction. This background was measured to be 1.5 ± 0.1 counts per minute. Protons lost between counters 3 and 4 by nuclear interactions, scattering, etc., may give some very small background to the deuterons and at the same time reduce the number of protons. No correction has been made for this effect. Base line determinations, which

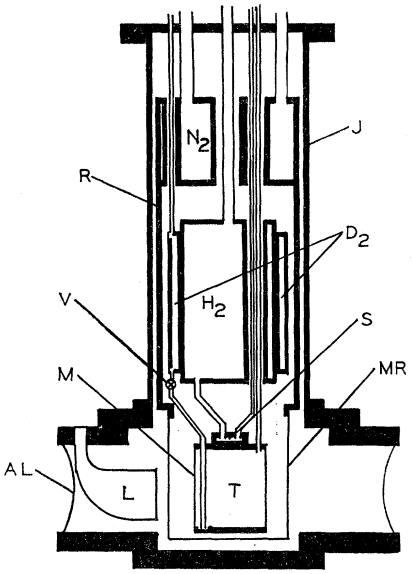

FIG. 5. Liquid deuterium target. The liquid deuterium target (T) was 1.4 g/cm² in thickness in a cylindrical Mylar container (M). Deuterium gas was liquified in a reservoir (D_2) which could be isolated from the target by a remote valve (V). The deuterium reservoir was a cylinder concentric with the liquid hydrogen reservoir (H_2) by which low temperature was maintained. The target itself was kept at liquid hydrogen temperature by means of a heat strap (S). The system was shielded from thermal radiation by a radiation shield (R) which at the target level was 0.5-mil gold-plated Mylar (MR). The radiation shield was in thermal contact with a liquid nitrogen reservoir (N_2). This whole system was in a vacuum jacket (J) which at beam height was a 12-mil aluminum window (AL). The liquid level could be observed visually by illuminating the target through a Lucite light pipe (L) and looking through a Mylar window (not shown).

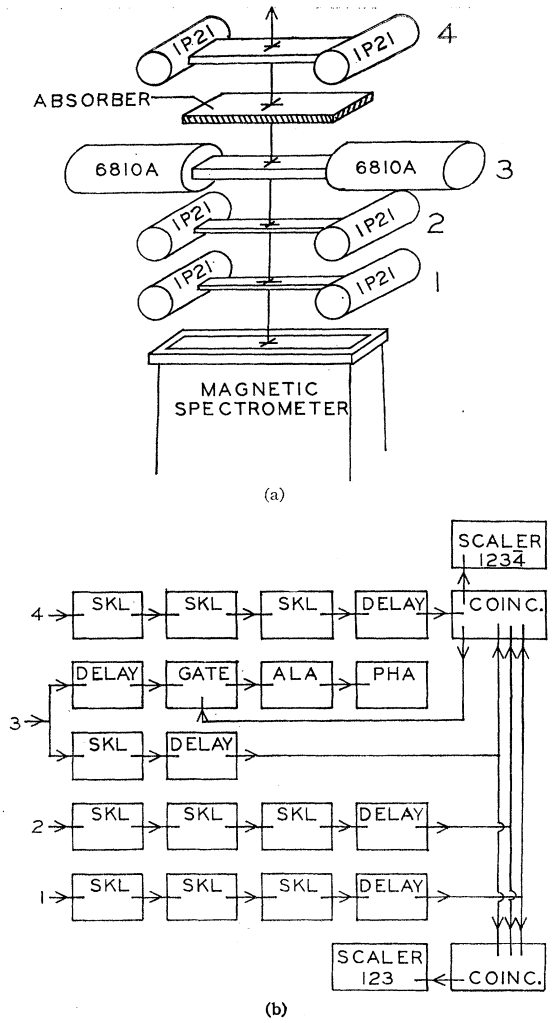

FIG. 6. (a) Counter telescope. (b) Electronics.

will be described later, showed some other real background contamination in the deuterons. This was observed and nearly eliminated by pulse-height analysis. Half of the number-3 counter pulse was fed into a 20 mμsec linear gate.[20] The gating pulse was a $123\bar{4}$ coincidence, which is the signature of a deuteron. The output pulse of the gate was fed into an Atomic linear amplifier (ALA). The output of the linear amplifier was fed into a 50-channel pulse-height analyzer[21] (PHA). The pulse-height analyzer was externally triggered by the discriminator output of the linear amplifier. A typical plot of the number of $123\bar{4}$ gated pulses against channel in the pulse-height analyzer is given in Fig. 7. Pulse-height analysis indicates that the residual deuteron background is really deuterons, probably from the empty target. For some angles the deuteron had sufficiently large a range that it could not be stopped in

[20] E. L. Garwin, Rev. Sci. Instr. **30**, 373 (1959).
[21] E. L. Garwin and A. Penfold, Chicago Synchrocyclotron internal report (unpublished).

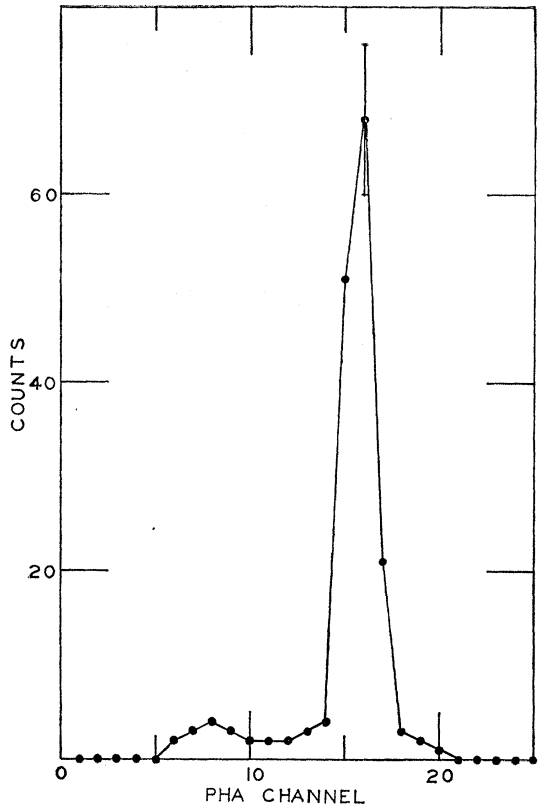

FIG. 7. PHA deuteron selection for $123\bar{4}$ gated pulses.

any absorber which we were able to provide. In these cases, 123 coincidences were used to identify deuterons instead of $123\bar{4}$'s. A typical plot of the number of 123 gated pulses against channel in the pulse-height analyzer in such a case is given in Fig. 8.

10. SEPARATION OF ELASTIC AND INELASTIC EVENTS

The separation of elastic from inelastic events was accomplished by means of the magnetic spectrometer. Since the deuterons are from purely elastic scattering and the counting statistics for deuterons are better than for protons, the recoil deuterons, or both protons and deuterons, were used whenever possible. A plot of the number of deuterons against momentum (Fig. 9) over a *p-d* peak is expected to be symmetric. Each point on the curve represents the sum of the counts in channels in which deuterons appear in the pulse-height analyzer (Figs. 7 and 8), for a given magnet current setting (momentum), for a fixed number of incident beam protons. A base line was established to eliminate the effect of the background. In the case of protons, (Fig. 10) the scattering has an inelastic component and the plot of number of protons against momentum is not symmetric. By symmetrizing the peak, the elastic component can be found. The area under these curves is a measure of the *p-d* elastic scattering intensity.

11. ERRORS

The errors quoted are statistical. Base lines were determined, where a sufficient number of points were available, by a least squares fit to a straight line. The error on the base line was taken as the root-mean-square deviation from the straight line.

12. EXPERIMENTAL LIMITATIONS

In Fig. 11 some kinematics appropriate to 420-Mev *p-d* scattering have been plotted. At laboratory angles greater than 65° the momentum of the deuterons is such that their range is too small to go through the counter telescope. This corresponds to proton center-of-mass angles less than 47.9°. Therefore, for smaller angles protons must be used. Elastically scattered protons at angles larger than 141° also have momentum such that their range is too small to go through the counter telescope. This corresponds to center-of-mass angles greater than 160°. Above 1150-Mev/c momentum, the coils of the magnet become hazardously hot. This prevents measurements of deuterons at angles less than 21° in the laboratory which is equivalent to protons of center-of-mass angle 135° or greater. The

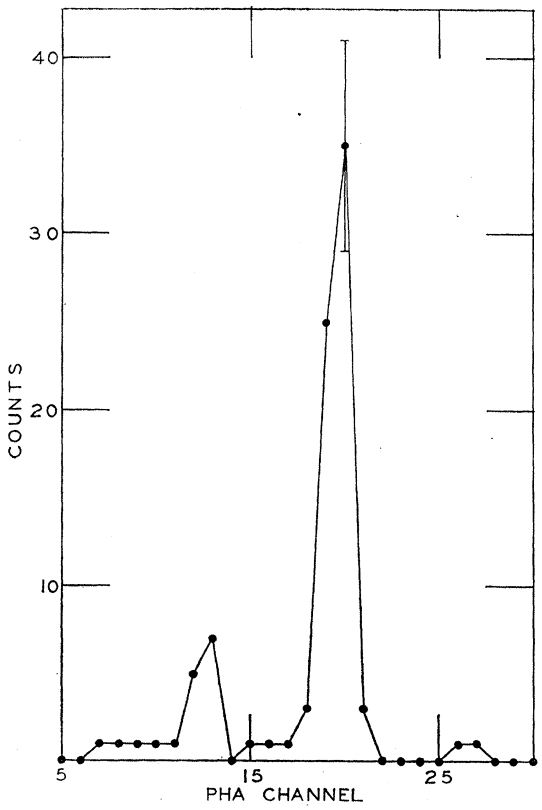

FIG. 8. PHA deuteron selection for 123 gated pulses. The separation of protons (channels 12 and 13) and deuterons can be seen.

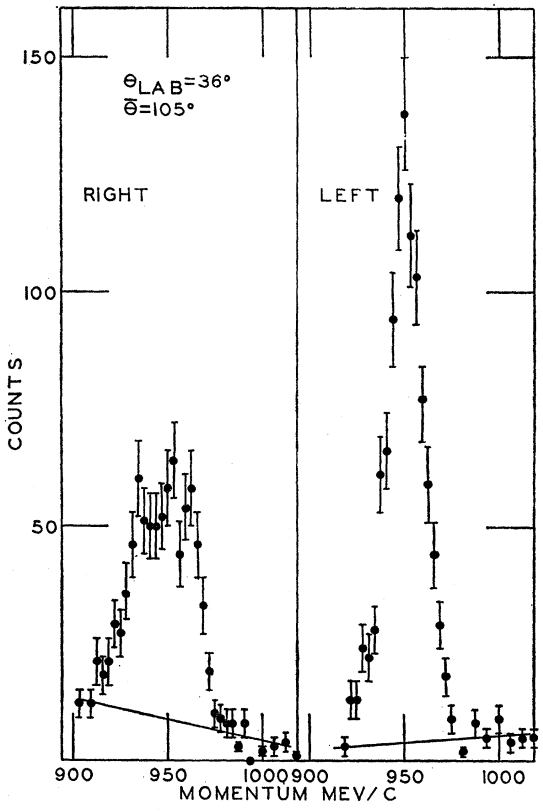

FIG. 9. Typical deuteron peak. The base lines shown are least-squares fits to a straight line of the base-line points. The large asymmetry can be seen from the difference in peak heights for deuterons scattered to the right from those scattered to the left.

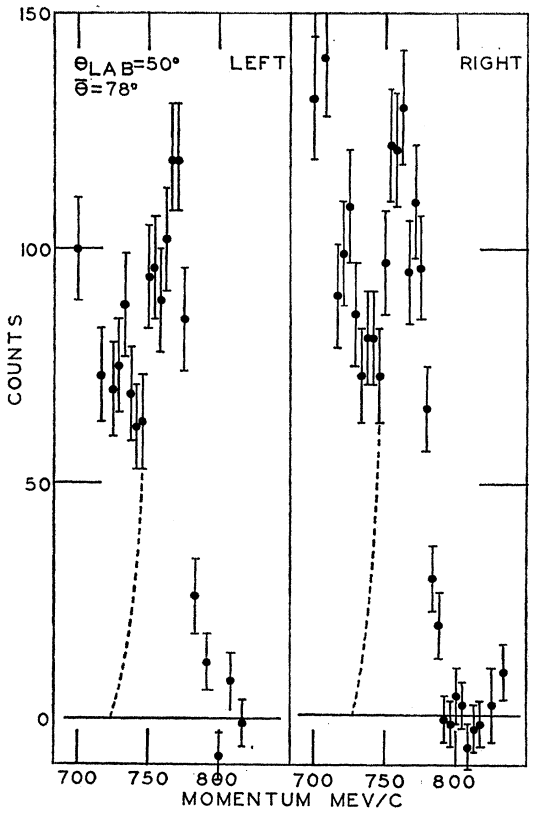

FIG. 10. Typical proton peak. The base lines shown are from averages of the base-line points. That the peaks are asymmetric due to the inelastic component is easily seen. The dotted lines indicate the low-momentum part of the symmetrized peaks. The asymmetry at this angle is small as can be seen from the similarity of the peak heights.

use of elastically scattered protons at large laboratory angles is restricted for two reasons:

(1) The intensity is very small due to the coupling of the already small cross section with the unfavorable solid angle conversion.

(2) The inelastic component in the scattering becomes worse at large angles.

The 135° maximum center-of-mass angle which can be reached with deuterons is, therefore, the experimental limit. In the experiment described here, the liquid deuterium, which was the same as was used in reference 10, was badly contaminated with hydrogen. The energy spread of the beam produced large mo-

TABLE I. Experimental results. The measured asymmetries and inferred polarizations are given for proton center-of-mass angles $\bar{\theta}$ and laboratory angles θ. The particle detected and its electronic signature are also given. The order in which measurements were made is indicated. The use of the PHA (Yes) or scalars (No) for registering the results is also indicated.

Proton c.m. angle $\bar{\theta}$	Asymmetry $\epsilon=P_1P_2$	Polarization P_2	Lab angle θ	Particle detected	Chrono-logical order	Gate pulse or signal	PHA
47.9	−0.056±0.032	−0.092±0.058	65°	d	V	$123\bar{4}$	Yes
59	−0.309±0.031	−0.502±0.058	59.1°	d	II	$123\bar{4}$	No
68	−0.358±0.048	−0.583±0.081	54.5°	d	VII	$123\bar{4}$	Yes
77.5	−0.100±0.037	−0.141±0.056	50°	d	I	$123\bar{4}$	No
78	−0.058±0.056		50°	p	I	123	No
90	−0.075±0.067	−0.122±0.111	59.1°	p	II	123	No
97	−0.069±0.53	−0.150±0.059	65°	p	V	123	No
97	−0.105±0.039		40°	d	III	123	No
105	−0.190±0.042	−0.309±0.073	36°	d	VI	123	Yes
115	+0.107±0.032	+0.174±0.059	31°	d	IV	123	No

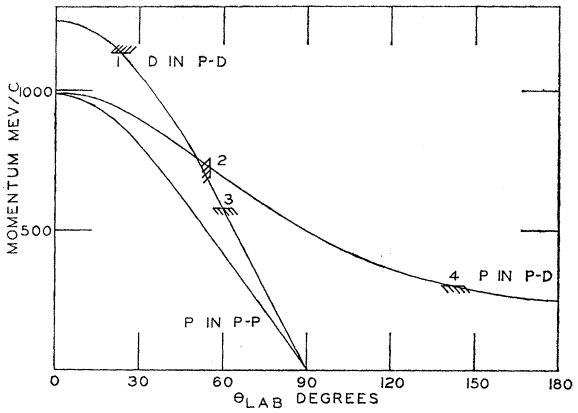

FIG. 11. Experimental limitations. The kinematics for elastic p-p and p-d scattering are plotted. 1 represents the highest current that the magnet can safely be run. 2 is the smallest angle at which the p in p-d can be separated from the p-p peak from the large hydrogen contamination. 3 is the smallest momentum for which the deuteron could penetrate the counter telescope. 4 is the smallest momentum for which protons could penetrate the counter telescope. The large inelastic component actually prevented the use of protons for all large angles.

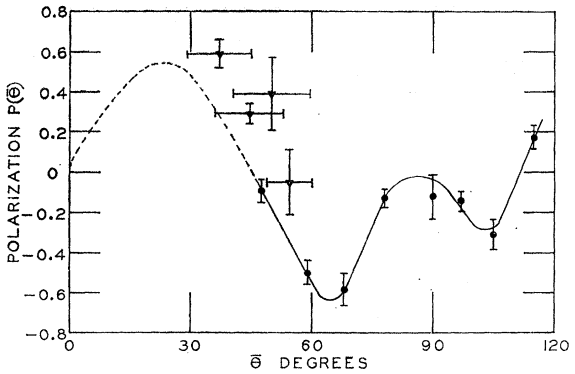

FIG. 12. Elastic p-d polarization. The triangular points are the 340-Mev points of reference 10. The circular points are the experimental 419-Mev points. The solid line is drawn only to guide the eye. The dashed line is the shape which is expected for the small angles at which the polarization has not yet been measured.

mentum peak widths. Therefore, in regions where they were close in momentum, the larger p-p peaks swamped the smaller elastic proton p-d peaks. This prevented the use of elastically scattered protons from p-d collisions at center-of-mass angles less than 78°. The angular region below 47.9°, as has been stated previously, could not be overlapped by deuteron measurements. Plans are being made to do these measurements in the near future with purer deuterium. The measurements in the present experiment were, therefore, limited to from 47.9° to 135° in the center-of-mass system.

13. RESULTS

The elastic p-d scattering intensity at each angle was measured first on one side of the beam and then on the other (Figs. 9 and 10). The asymmetry ϵ is given by equation 8 for protons and by

$$\epsilon=(R-L)/(L+R) \tag{9}$$

for deuterons, since the proton and deuteron go in opposite directions in the center-of-mass system. The results are given in Table I. A plot of the elastic p-d polarization as a function of center-of-mass angle is given in Fig. 12. The 340-Mev points of reference 10 are also plotted. The general shape of the curve out to 90° center of mass is the same as is predicted by the 300-Mev phase shifts at 300 Mev. The negative dip at 105°, outside the range of the theoretical analysis discussed, was unexpected. Since the polarization must return to zero at 180°, there is at least one additional polarization maximum between 110° and 180°. A positive maximum is expected, though not yet measured, between 20° and 30°. Any choice of 420-Mev N-N phase shifts must, when used in the calculation of the elastic p-d polarization give (1) a zero near 45°, (2) a large minimum near 65°, (3) a small negative maximum somewhere between 80° and 95°, and (4) a negative decreasing polarization thereafter. The magnitudes of the elastic p-d polarization measured in this experiment and the value of the maximum between 20° and 30° will permit a calculation of the $I=0$ n-p phase shifts when a satisfactory set of $I=1$ N-N phase shifts is made available. The points (1) through (4) mentioned above are rather strong requirements for any complete set of N-N phase shifts.

Plans are being made to extend these measurements to lower angles and to measure the elastic p-d polarization in the 300-Mev region.

ACKNOWLEDGMENTS

Thanks are due to Dr. Albert V. Crewe, the author's sponsor, for his encouragement and helpful discussions. Endre Lillethun, Robert March, and Charles Rey deserve recognition for their assistance during this three week long Cyclotron run. Thanks also go to Richard Arnold, Manfred Pyka, and Joseph Lenko for their help with the liquid deuterium target.

APPENDIX

Letting

$$\lambda_1=\tfrac{1}{4}(B+G+N),\quad \lambda_2=C,\quad \lambda_3=\tfrac{1}{4}(G+2H-B-N),\quad \lambda_4=\tfrac{1}{4}(G-2H-B-N),\quad \text{and}\quad \lambda_5=\tfrac{1}{4}(3N-B-G),^{21a}$$

the λ_i are given for the p-p case by[22]

[21a] *Note added in proof.*—Corrected expressions were provided by Y. Sakamoto, Kyoto University, Kyoto, Japan.

[22] S. C. Wright, Phys. Rev. **99**, 996 (1955).

$$B=-\frac{\alpha}{2k'}e^{2i\eta_0}[\mathcal{S}+\mathcal{C}]+\frac{1}{ik'}\sum_{\text{even } l}(2l+1)\alpha_{l,0}{}^N e^{2i\eta_l}P_l,$$

$$C=\frac{\sin\bar\theta'}{4k'}\left\{\sum_{\text{odd } l}\left[\frac{(2l+3)}{l+1}\beta_1{}^{l+1}P_l'-\frac{(2l+3)}{l+2}\beta_2{}^{l+1}P_{l+2}'-\frac{(2l+1)}{l(l+1)}\alpha_{l,1}{}^N e^{2i\eta_l}P_l'\right]-\alpha_{0,1}{}^N e^{2i\eta_1}\right\},$$

$$N=-\frac{\alpha}{2k'}e^{2i\eta_0}[\mathcal{S}-\mathcal{C}]+\frac{1}{2ik'}\left\{\sum_{\text{odd } l}\left[\beta_1{}^{l+1}\left(2(l+1)P_l-\frac{\cos\bar\theta'}{l+1}P_l'\right)+\beta_2{}^{l+1}\left(2(l+2)P_{l+2}-\frac{\cos\bar\theta'}{l+2}P_{l+2}'\right)\right.\right.$$
$$\left.\left.-\frac{1}{[(l+1)(l+2)]^{\frac{1}{2}}}\beta_3{}^{l+1}P_{l+1}'+\frac{(2l+1)}{l(l+1)}\cos\bar\theta'\alpha_{l,1}{}^N e^{2i\eta_l}P_l'\right]+\alpha_{0,1}{}^N e^{2i\eta_1}P_1\right\},$$

$$H=\frac{1}{2ik'}\left\{\sum_{\text{odd } l}\left[\frac{1}{l+1}\beta_1{}^{l+1}P_l'+\frac{1}{l+2}\beta_2{}^{l+1}P_{l+2}'+\frac{1}{[(l+1)(l+2)]^{\frac{1}{2}}}\beta_3{}^{l+1}(\cos\bar\theta'P_{l+1}'-2(l+2)(l+1)P_{l+1})\right.\right.$$
$$\left.\left.-\frac{(2l+1)}{l(l+1)}\alpha_{l,1}{}^N e^{2i\eta_l}P_l'\right]+\alpha_{0,1}{}^N e^{2i\eta_1}\right\},$$

$$G-N=-\frac{\alpha}{2k'}e^{2i\eta_0}[\mathcal{S}-\mathcal{C}]+\frac{1}{ik'}\left\{\sum_{\text{odd } l}\left[\beta_1{}^{l+1}\left(P_l+\frac{\cos\bar\theta'}{l+1}P_l'\right)+\beta_2{}^{l+1}\left(-P_{l+2}+\frac{\cos\bar\theta'}{l+2}P_{l+2}'\right)\right.\right.$$
$$\left.\left.+\frac{1}{[(l+1)(l+2)]^{\frac{1}{2}}}\beta_3{}^{l+1}P_{l+1}'+(2l+1)\alpha_{l,1}{}^N e^{2i\eta_l}\left(P_l-\frac{\cos\bar\theta'}{l(l+1)}P_l'\right)\right]\right\},$$

where $P_l'=dP_l/d\cos\bar\theta'$, P_l is the Legendre polynomial of order l,

$$e^{2i\eta_l}=\Gamma(l+1+i\alpha)/\Gamma(l+1-i\alpha),\quad \alpha=e^2/\hbar v.$$

η_l is the Coulomb phase shift. $\alpha_{j,1}{}^N e^{2i\eta_l}=e^{2i\delta_{lj}}-e^{2i\eta_l}$; δ_{lj} is the triplet phase shift[23] of orbital momentum l and total angular momentum j. $\alpha_{l,0}{}^N e^{2i\eta_l}$ is the corresponding quantity for singlet states with phase shift $\delta_{l=j}$.

$$\beta_1{}^j=[\exp(2i\delta_{j-1,j})-\exp(2i\eta_{j-1})]\cos^2\epsilon_j+[\exp(2i\delta_{j+1,j})-\exp(2i\eta_{j-1})]\sin^2\epsilon_j;$$

ϵ_j is the mixing parameter for mixing states with equal total angular momentum j and orbital angular momenta $j+1$ and $j-1$.

$$\beta_2{}^j=[\exp(2i\delta_{j-1,j})-\exp(2i\eta_{j+1})]\sin^2\epsilon_j+[\exp(2i\delta_{j+1,j})-\exp(2i\eta_{j+1})]\cos^2\epsilon_j,$$
$$\beta_3{}^j=[\exp(2i\delta_{j-1,j})-\exp(2i\delta_{j+1,j})]\sin 2\epsilon_j.$$

For the n-p case the same formulas apply with α put equal to zero and the sums extended over all l save the absent $^3S_0$ state. Since charge independence is assumed, there is no mixing between the singlet and triplet states.[24]

Carrying out these summations to H waves,[6] for the p-p case

$$B=f_c(\bar\theta')+f_c(\pi-\bar\theta')+\frac{1}{8ik'}\{[8\alpha_0-20\alpha_2+27\alpha_4]+[60\alpha_2-270\alpha_4]\cos^2\bar\theta'+315\alpha_4\cos^4\bar\theta'\},$$

$$C=-\frac{\sin\bar\theta'}{64k'}\{[16\alpha_{10}+24\alpha_{11}-40\alpha_{12}-40\alpha_{32}-14\alpha_{33}+54\alpha_{34}+54\alpha_{54}+11\alpha_{55}-65\alpha_{56}]+[200\alpha_{32}+70\alpha_{33}-270\alpha_{34}$$
$$-756\alpha_{54}-154\alpha_{55}+910\alpha_{56}]\cos^2\bar\theta'+[1134\alpha_{54}+231\alpha_{55}-1365\alpha_{56}]\cos^4\bar\theta'\},$$

$$H=\frac{1}{32ik'}\{[16\alpha_{10}-24\alpha_{11}+8\alpha_{12}-8\alpha_{32}+14\alpha_{33}-6\alpha_{34}+6\alpha_{54}-11\alpha_{55}+5\alpha_{56}-32(6)^{\frac{1}{2}}\alpha^2+48(5)^{\frac{1}{2}}\alpha^4]$$
$$+[40\alpha_{32}-70\alpha_{33}+30\alpha_{34}-84\alpha_{54}+154\alpha_{55}-70\alpha_{56}+80(6)^{\frac{1}{2}}\alpha^2-456(5)^{\frac{1}{2}}\alpha^4]\cos^2\bar\theta'$$
$$+[126\alpha_{54}-231\alpha_{55}+105\alpha_{56}+504(5)^{\frac{1}{2}}\alpha^4]\cos^4\bar\theta'\},$$

[23] J. M. Blatt and L. C. Biedenharn, Revs. Modern Phys. **24**, 258 (1952).
[24] R. H. Dalitz, Proc. Phys. Soc. (London) **A65**, 175 (1952).

$$N=f_c(\bar\theta')-f_c(\pi-\bar\theta')+\frac{1}{32ik'}\{[16\alpha_{10}+24\alpha_{11}+56\alpha_{12}-136\alpha_{32}-14\alpha_{33}-186\alpha_{34}+294\alpha_{54}+11\alpha_{55}+355\alpha_{56}$$
$$+16(6)^{\frac{1}{2}}\alpha^2-24(5)^{\frac{1}{2}}\alpha^4]\cos\bar\theta'+[200\alpha_{32}+70\alpha_{33}+290\alpha_{34}-1316\alpha_{54}-154\alpha_{55}-1610\alpha_{56}+56(5)^{\frac{1}{2}}\alpha^4]\cos^3\bar\theta'$$
$$+[1134\alpha_{54}+231\alpha_{55}+1407\alpha_{56}]\cos^5\bar\theta'\},$$
$$G-N=f_c(\bar\theta')-f_c(\pi-\bar\theta')+\frac{1}{32ik'}\{[48\alpha_{11}+48\alpha_{12}+32\alpha_{32}-308\alpha_{33}-60\alpha_{34}-48\alpha_{54}+638\alpha_{55}+70\alpha_{56}-32(6)^{\frac{1}{2}}\alpha^2$$
$$+48(5)^{\frac{1}{2}}\alpha^4]\cos\bar\theta'+[420\alpha_{33}+140\alpha_{34}+112\alpha_{54}-2772\alpha_{55}-420\alpha_{56}-112(5)^{\frac{1}{2}}\alpha^4]\cos^3\bar\theta'$$
$$+[2310\alpha_{55}+462\alpha_{56}]\cos^5\bar\theta'\},$$
$$f_c(\bar\theta')=-\frac{\alpha}{k'(1-\cos\bar\theta')}\exp\{-i\alpha\ln[\tfrac{1}{2}(1-\cos\bar\theta')]\}.$$

Using bar phase shifts,[5]

$$\alpha_l=\exp(2i\bar\delta_l)-\exp(2i\Phi_l),\quad \Phi_l\equiv\eta_l-\eta_0=\sum_{x=1}^{l}\arctan\left(\frac{\alpha}{x}\right);$$

$$\alpha_{lj}=\cos2\bar\epsilon_j\exp(2i\bar\delta_{lj})-\exp(2i\Phi_l),\quad \alpha^j=i\sin2\bar\epsilon_j\exp[i(\bar\delta_{j+1,j}+\bar\delta_{j-1,j})].$$

This may be compared to the previous notation, $\alpha_{l,0}{}^N e^{2i\Phi_l}=\alpha_l$, $\beta_1{}^j=\alpha_{j-1,j}$, $\beta_2{}^j=\alpha_{j+1,j}$, $\beta_3{}^j=-2\alpha^j$, and $\alpha_{j,1}{}^N e^{2i\Phi_l}=\alpha_{lj}$ for uncoupled triplet states. For the *n-p* case, with α set equal to zero,

$$B=\frac{1}{8ik'}\{[8\alpha_0-20\alpha_2+27\alpha_4]+[24\alpha_1-84\alpha_3+165\alpha_5]\cos\bar\theta'+[60\alpha_2-270\alpha_4]\cos^2\bar\theta'$$
$$+[140\alpha_3-770\alpha_5]\cos^3\bar\theta'+315\alpha_4\cos^4\bar\theta'+693\alpha_5\cos^5\bar\theta'\},$$
$$C=-\frac{\sin\bar\theta'}{64k'}\{[16\alpha_{10}+24\alpha_{11}-40\alpha_{12}-40\alpha_{32}-14\alpha_{33}+54\alpha_{34}+54\alpha_{54}+11\alpha_{55}-65\alpha_{56}]+[72\alpha_{21}+40\alpha_{22}-112\alpha_{23}$$
$$-210\alpha_{43}-54\alpha_{44}+264\alpha_{45}]\cos\bar\theta'+[200\alpha_{32}+70\alpha_{33}-270\alpha_{34}-756\alpha_{54}-154\alpha_{55}+910\alpha_{56}]\cos^2\bar\theta'$$
$$+[490\alpha_{43}+126\alpha_{44}-616\alpha_{45}]\cos^3\bar\theta'+[1134\alpha_{54}+231\alpha_{55}-136\alpha_{56}]\cos^4\bar\theta'\},$$
$$N=\frac{1}{32ik'}\{[32\alpha_{01}-32\alpha_{21}-48\alpha_{23}+48\alpha_{43}+60\alpha_{45}+16\sqrt{2}\alpha^1-8\sqrt{3}\alpha^3]+[16\alpha_{10}+24\alpha_{11}+56\alpha_{12}-136\alpha_{32}-14\alpha_{33}$$
$$-186\alpha_{34}+294\alpha_{54}+11\alpha_{55}+355\alpha_{56}+16(6)^{\frac{1}{2}}\alpha^2-24(5)^{\frac{1}{2}}\alpha^4]\cos\bar\theta'+[72\alpha_{21}+40\alpha_{22}+128\alpha_{23}-450\alpha_{43}-54\alpha_{44}$$
$$-576\alpha_{45}+40\sqrt{3}\alpha^3]\cos^2\bar\theta'+[200\alpha_{32}+70\alpha_{33}+290\alpha_{34}-1316\alpha_{54}-154\alpha_{55}-1610\alpha_{56}+56(5)^{\frac{1}{2}}\alpha^4]\cos^3\bar\theta'$$
$$+[490\alpha_{43}+126\alpha_{44}+644\alpha_{45}]\cos^4\bar\theta'+[1134\alpha_{54}+231\alpha_{55}+1407\alpha_{56}]\cos^5\bar\theta'\},$$
$$H=\frac{1}{32ik'}\{[16\alpha_{10}-24\alpha_{11}+8\alpha_{12}-8\alpha_{32}+14\alpha_{33}-6\alpha_{34}+6\alpha_{54}-11\alpha_{55}+5\alpha_{56}-32(6)\alpha^2+48(5)^{\frac{1}{2}}\alpha^4]+[24\alpha_{21}-40\alpha_{22}$$
$$+16\alpha_{23}-30\alpha_{43}+54\alpha_{44}-24\alpha_{45}+48\sqrt{2}\alpha^1-184\sqrt{3}\alpha^3]\cos\bar\theta'+[40\alpha_{32}-70\alpha_{33}+30\alpha_{34}-84\alpha_{54}+154\alpha_{55}-70\alpha_{56}$$
$$+80(6)^{\frac{1}{2}}\alpha^2-456(5)^{\frac{1}{2}}\alpha^4]\cos^2\bar\theta'+[70\alpha_{43}-126\alpha_{44}+56\alpha_{45}+280\sqrt{3}\alpha^3]\cos^3\bar\theta'$$
$$+[126\alpha_{54}-231\alpha_{55}+105\alpha_{56}+504(5)^{\frac{1}{2}}\alpha^4]\cos^4\bar\theta'\},$$
$$G-N=\frac{1}{32ik'}\{[32\alpha_{01}+16\alpha_{21}-80\alpha_{22}-16\alpha_{23}-12\alpha_{43}+108\alpha_{44}+12\alpha_{45}-32\sqrt{2}\alpha^1+16\sqrt{3}\alpha^3]+[48\alpha_{11}+48\alpha_{12}+32\alpha_{32}$$
$$-308\alpha_{33}-60\alpha_{34}-48\alpha_{54}+638\alpha_{55}+70\alpha_{56}-32(6)^{\frac{1}{2}}\alpha^2+48(5)^{\frac{1}{2}}\alpha^4]\cos\bar\theta'+[160\alpha_{22}+80\alpha_{23}+60\alpha_{43}-972\alpha_{44}$$
$$-168\alpha_{45}-80\sqrt{3}\alpha^3]\cos^2\bar\theta'+[420\alpha_{33}+140\alpha_{34}+112\alpha_{54}-2772\alpha_{55}-420\alpha_{56}-112(5)^{\frac{1}{2}}\alpha^4]\cos^3\bar\theta'$$
$$+[1008\alpha_{44}+252\alpha_{45}]\cos^4\bar\theta'+[462\alpha_{56}+2310\alpha_{55}]\cos^5\bar\theta'\}.$$